We are IntechOpen, the world's leading publisher of Open Access books
Built by scientists, for scientists

5,600
Open access books available

137,000
International authors and editors

170M
Downloads

Our authors are among the

154
Countries delivered to

TOP 1%
most cited scientists

12.2%
Contributors from top 500 universities

CLARIVATE ANALYTICS
BOOK CITATION INDEX
INDEXED

WEB OF SCIENCE™

Selection of our books indexed in the Book Citation Index in Web of Science™ Core Collection (BKCI)

Interested in publishing with us?
Contact book.department@intechopen.com

Numbers displayed above are based on latest data collected.
For more information visit www.intechopen.com

Chapter

Experimental Investigations on Fuel Spray and Impingement for Gasoline Direct Injection Engines

Hongliang Luo

Abstract

Spray-wall impingement is a widespread phenomenon applied in many fields, including spray-wall cooling system, spray coating process and fuel spray and atomization in internal combustion engines. In direct-injection spark ignition (DISI), it is difficult to avoid the fuel film on the piston head and cylinder surfaces. The wet wall caused by impingement affects the air-fuel mixture formation process, which finally influence the subsequent combustion efficiency and performance. Therefore, the fuel spray and impingement under gasoline engine-like conditions were characterized. Mie scattering technique was applied to visualize the spray evolution and impingement processes in a high-pressure and high-temperature constant chamber. Meanwhile, the adhered fuel film on the wall was measured by refractive index matching (RIM) under non-evaporation and evaporation conditions considering the effects of different injection pressures, ambient pressures and ambient temperatures. Additionally, the fuel film formation and evaporation evolution models were proposed with the help of these mechanisms.

Keywords: fuel spray, impingement, fuel film, non-evaporation and evaporation

1. Introduction

Generally, compared to port fuel injection (PFI) engine, direct-injection spark ignition (DISI) engines as a greatly potential alternative become more and more widely used for their significant advantages [1, 2]. However, owing to the short impingement distance and high injection pressure, spray impingement on the cylinder wall and piston head is quite difficult to avoid. The impingement affects the fuel-air mixture prior to combustion, which is a possible source for unburned hydrocarbon (UHC) and particulate matters (PM) [3]. Tanaka et al. [4] showed the relationship between the deterioration ratio of engine particle number (PN) emissions and fuel film volume, indicating that PN emissions increases with the increasing of fuel film on the wall.

As we known, when fuel immediately out of the nozzle hole, the spray breakup occurs. Two processes of fuel breakup can be involved. The first breakup is also called the primary breakup, leading to large droplets and liquid ligaments near the nozzle to form the dense spray [5, 6]. Under the high injection pressure condition, the cavitation and turbulence are generated from the injector holes, which should be the main reason for this mechanism. Then the following breakup process is named as secondary breakup, indicating these existing droplets break up into

smaller ones owing to aerodynamic forces caused by the relative velocity between droplets and surrounding ambient gas. During the secondary break-up, more and more liquid droplets are formed and move downstream of the spray. Although considerable researches were done for the spray and atomization mechanisms, the spray and impingement are less discussed, let along the fuel film formation after impingement. By considering the competitions from the pure electric vehicle (EV) and concerns on environmental pollution, it is urgent to understand the interaction of liquid droplet and piston wall thoroughly to improve the spray atomization in engine work process.

The target of this study is to investigate the characteristics of gasoline spray impingement and fuel film formation experimentally. The specific objectives of this study are shown as follows:

- Analyze the impinging spray evolution characteristics which belongs to the single-hole nozzle under the non-evaporation and evaporation conditions.

- Model the fuel film formation to provide an insightful understanding of the interaction between spray and wall.

In this study, Mie Scattering technique was implemented to obtain the observations of gasoline spray emerging from single hole injector under different conditions. RIM technique was adopted to analyze the formation process of fuel liquid on the wall qualitatively and quantitatively under both non-evaporation and evaporation conditions.

2. Experimental apparatus and measurement methods

As shown in **Figure 1**, a quartz glass (Sigma Koki, DFSQ1-50CO2) was used as the impingement wall with a diameter at 50 mm and thickness at 2 mm.

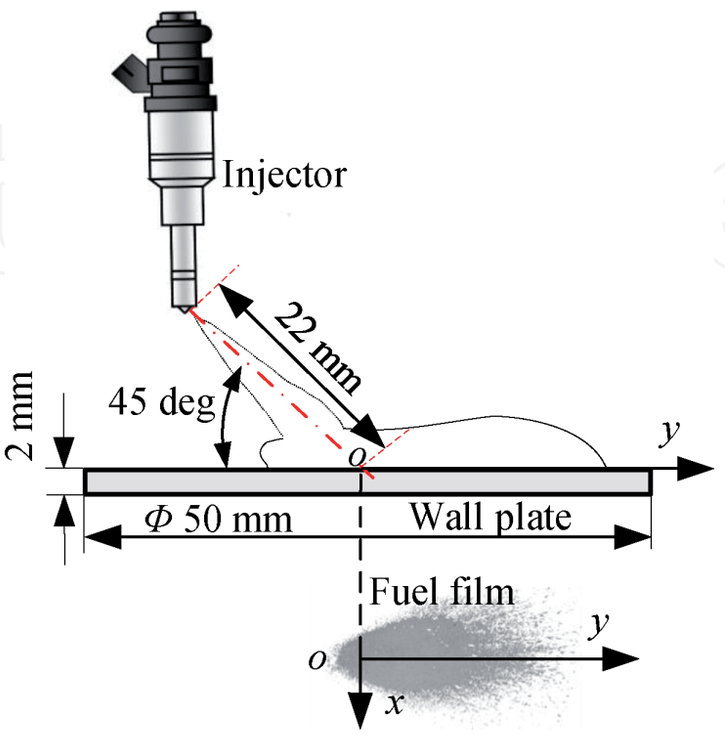

Figure 1.
Schematic of injector and flat wall.

The coordinate system is established and defined, and the intersection point *o* of the nozzle center axis and the flat wall is decided as the impingement point. The positive *y* axis is along the lateral direction of the spray after impingement, and the positive *x* axis is pointing out of the figure. The impingement angle was 45 deg. and the impingement distance was 22 mm from the nozzle exit to the impingement point of the flat wall along the spray axis. Moreover, the surface roughness was measured at Ra 7.0 μm by a portable high-performance surface roughness and waviness measuring instrument (Kosaka Laboratory Ltd., SE300).

The experiment was performed in a constant high-pressure chamber filled with nitrogen gas. A single hole mini-sac injector was used with length at 0.65 mm and hole diameter at 0.155 mm. The test conditions are listed in **Table 1**. Toluene was selected as a substitute for gasoline. The fuel temperature (before injection) was regulated by a cooling system to maintain it at room temperature. The injection pressure changes among 10, 20 and 30 MPa, resulting in the different duration at 2.9, 2.1, and 1.7 ms for fuel injection, which satisfies the constant injection mass at 4.0 mg by considering the real injection mass in each hole. In order to study the influence of ambient pressure, pressures between 0.15 and 0.74 MPa were tested at evaporation condition (T_{amb} = 433 K). Meanwhile, the equivalent non-evaporating conditions (P_{amb} = 0.1 MPa, T_{amb} = 298 K and P_{amb} = 0.5 MPa, T_{amb} = 298 K) were determined by maintaining the ambient density at 1.95 and 5.95 kg/m^3, respectively. One thing should be pointed out that the saturated temperatures (T_{sat}) of toluene under P_{amb} = 0.15 MPa is 398 K, and it is cleat to see that $T_{sat} < T_{amb}$. While under P_{amb} = 0.74 MPa, T_{sat} is 472 K, higher than T_{amb}.

2.1 Mie scattering method

In order to observe the spray development process, the Mie scatting experiment was performed, and the specific experimental apparatus are shown in **Figure 2**. A high-speed video camera (Photron FASTCAM SA-Z) was utilized to observe the spray with a frame rate at 20,000 frames per second (fps) and a frame size at 512 × 512 pixels. A xenon lamp (Ushio SX-131 UID501XAMQ) was set in a direction perpendicular to the camera to illuminate the spray, and it was placed in the same plane with the camera.

The spray tip penetration (S) and impinging spray height (H_i) are widely used to investigate the characteristics of the spray-wall impingement [7, 8]. These values were experimentally obtained from raw images by determining the edge of

	Non-evaporation conditions	Evaporation conditions
Test Fuel	Toluene	
Fuel Temperature	298 K	
Injection Mass	4.0 mg	
Ambient Gas	Nitrogen	
Injection Pressure	10, 20, 30 MPa	
Injection Duration	2.9, 2.1, 1.7 ms	
Ambient Temperature	298 K	433 K
Ambient Pressure	0.1 and 0.5 MPa	0.15 and 0.74 MPa
Ambient Density	1.95 and 5.95 kg/m^3	1.95 and 5.95 kg/m^3

Table 1.
Test conditions.

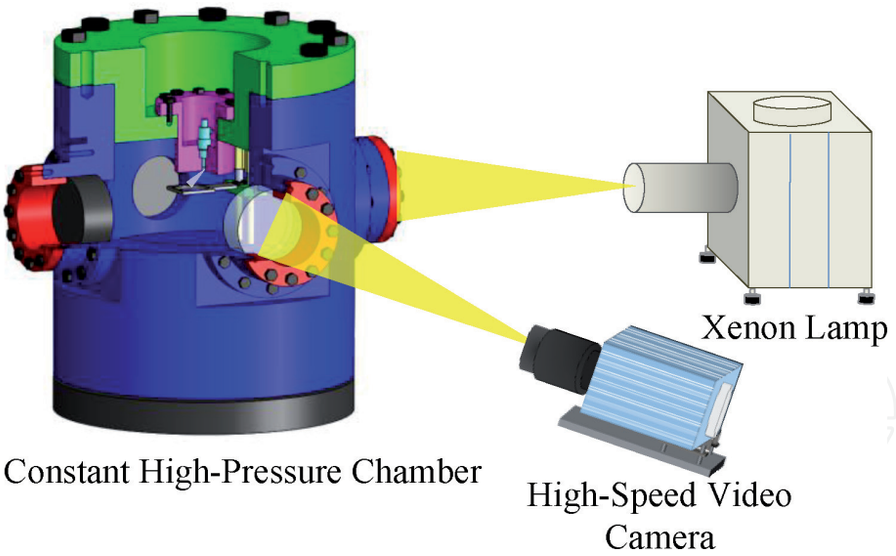

Figure 2.
Experimental apparatus.

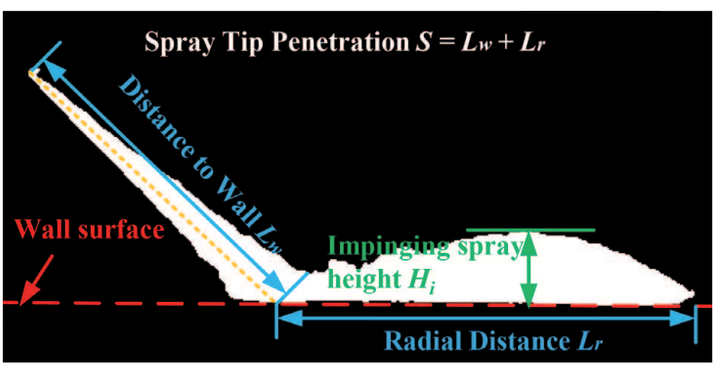

Figure 3.
Experimental extraction of S and H_i.

the impinging spray using inhouse code created in MATLAB software as shown in **Figure 3**. The dotted line represents the wall surface. S and H_i are defined. S is defined as the distance from the nozzle exit to the spray tip. Generally, before impingement, S is just the distance from the nozzle exit to the spray tip. However, after wall impingement, S is defined as the sum of the distance to wall (L_w) and the radial distance (L_r) [9]. H_i is the maximum distance from the wall surface to the edge of the impinging spray. All the results were calculated five times under each specific set of experimental conditions, and the average values were presented.

2.2 RIM method

The RIM experimental equipment in the current study is shown in **Figure 4**. Some differences can be found in the optical system with Mie scattering. The xenon lamp was placed at the side window to emit continuous light with an incident angle at 15 deg. Under the flat wall, a reflection mirror was positioned directly. Fuel film images were observed by a high-speed video camera through this mirror. Further, the high-speed video camera was set at a frame rate of 10,000 fps and at a frame size of 512 × 512 pixels.

RIM method is applied to measure the fuel film thickness. The image processing is shown in **Figure 5**. First, the image without fuel film named as "dry image" is acquired. After fuel adhering on the wall, it is subtracted by the "dry image"

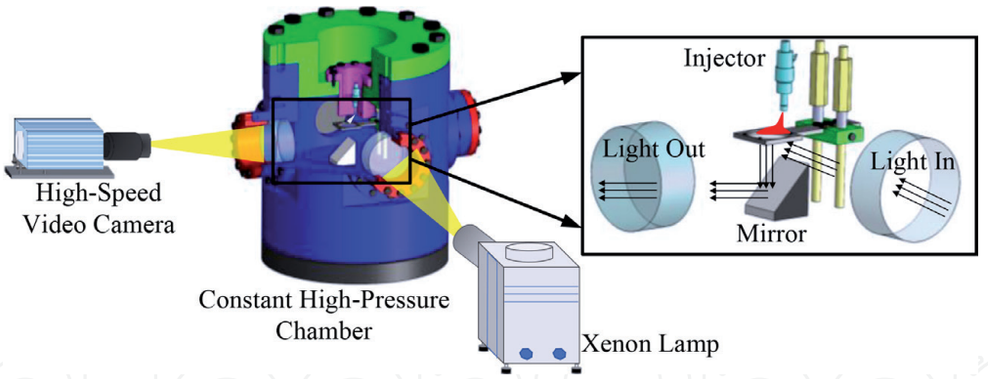

Figure 4.
Experimental setup for fuel film measurement.

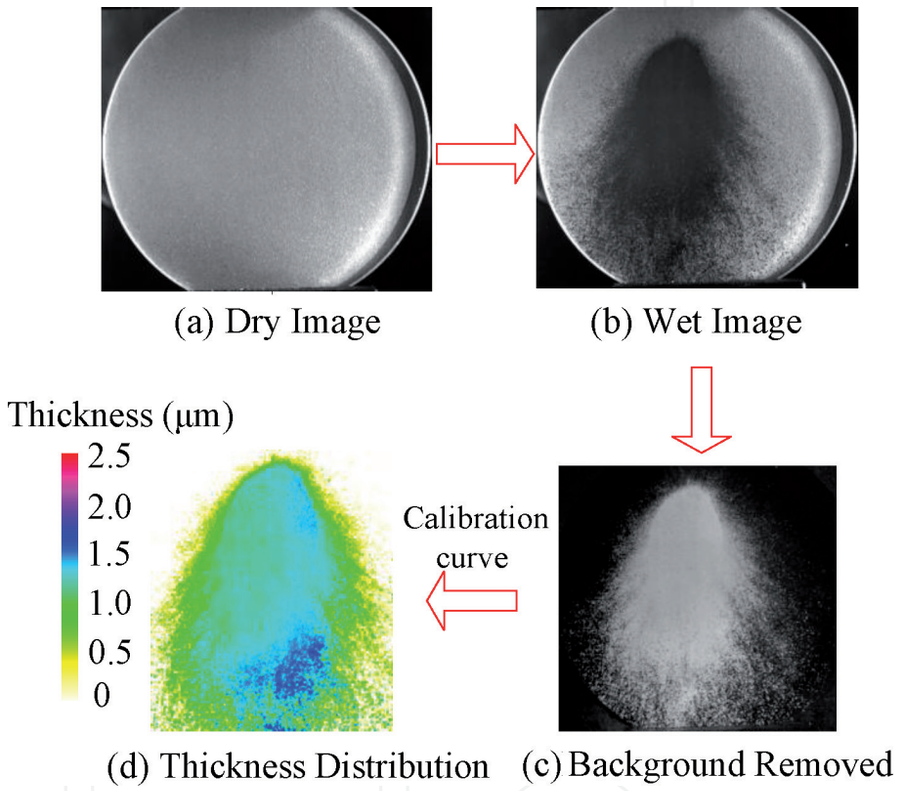

Figure 5.
Image processing.

to obtain the only adhered film image. Using the calibration result, the thickness distribution can be obtained. With the scale (0.106 mm/pixel) got from the observation, the film area is calculated by integrating the available pixels. While, for the mass, the thickness can be added up if larger than 0.1 μm. Then the film mass can be calculated through the scale and density of toluene (867 kg/m^3). Additional details about RIM method and calibration can be seen in the previous publications [10–13].

3. Impinging spray under evaporation conditions

3.1 Effect of temperature

To discuss the spray characteristics under different ambient temperatures, the images of spray and fuel film at 1.5 ms and 4.0 ms after start of injection (ASOI)

under T_{amb} = 298 K are presented in **Figure 6(a)**. The sprays are displayed as binary images acquired from the Mie scattering experiment, and the fuel films are shown in pseudo-color images obtained from the RIM experiment. During injection, the fuel film is incomplete and invalid owing to the mie scattering effect caused by the illumination of the droplets above the wall. While, the fuel film becomes complete and thus available after injection. Therefore, all the results related to the adhesion are shown and discussed after fuel injection. Besides, it is clear to see that the impinging spray height at 4.0 ms ASOI is a little larger than that at 1.5 ms ASOI. And more droplets accumulated at the downstream should be one possible reason for it. Furthermore, the fuel film at impingement region (called Region I) is thicker than that at the periphery region (called Region II) and the thickness decreases along y direction. This is due to different mechanisms in the formation of fuel film, which will be explained detailly in the following section.

The images of spray and fuel film at 1.5 ms and 4.0 ms ASOI under T_{amb} = 433 K can be seen in **Figure 6(b)**. Under condition of high ambient temperature, the impinging spray height is shorter than that under T_{amb} = 298 K, owing to the evaporation of fuel droplets. This phenomenon is more obvious at 4.0 ms AOSI. Moreover, the spray area is smaller in contrast to that observed under T_{amb} = 298 K, which can be also explained by the evaporation of droplets during spray. By comparing **Figure 6(a)** and **(b)**, it is evident that evaporation is more significant at the periphery than that observed on Region I.

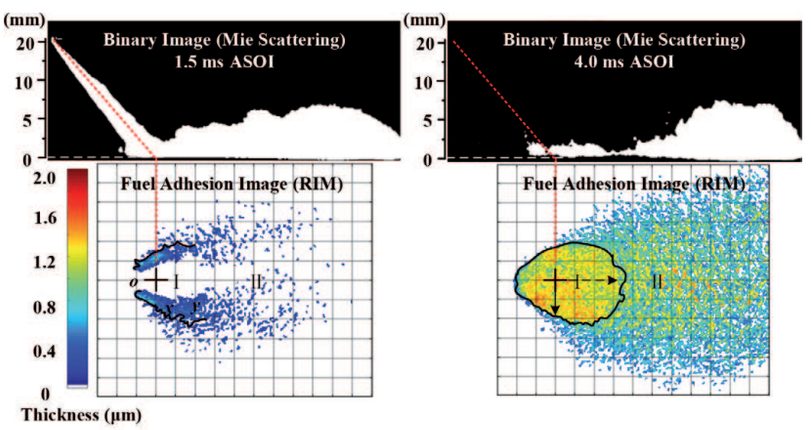

Figure 6.
Spray impingement and fuel film during and after injection. (a) T_{amb} = 298 K. (b) T_{amb} = 433 K.

For clarifying the effect of ambient temperature on fuel film thickness distribution along different lines, which were clearly defined to express them concisely. As illustrated in **Figure 7**, the coordinate system is created by setting the impingement point as the origin *o*. As fuel film is almost symmetric along the *y* axis, thickness distribution can be only discussed at different *y* lines at $y = -2.5$, 2.5, 7.5, and 12.5 mm, and the thickness at these lines was described as $H_{-2.5}$, $H_{2.5}$, $H_{7.5}$, and $H_{12.5}$, respectively. The results of $H_{-2.5}$, $H_{2.5}$, $H_{7.5}$, and $H_{12.5}$ at 5 and 50 ms ASOI under $T_{amb} = 298$ K and 433 K are depicted in **Figure 8**, respectively. The horizontal axis is from −15 to 15 mm, and the vertical axis denotes fuel film thickness.

The results at 5 ms ASOI are shown in **Figure 8(a)**. The thickness under $T_{amb} = 298$ K is larger than that under $T_{amb} = 433$ K due to non-evaporation. For all cases except of $H_{12.5}$, thickness distribution can be divided into three parts as "initially increases, remains constant, and finally decreases". For the constant value, $H_{-2.5}$ and $H_{2.5}$ under 298 K are similar to those under 433 K, but $H_{7.5}$ under 433 K is slightly smaller than that under 298 K. Then as the constant values under 298 K and 433 K are similar, this region is defined as Region I. While for the other region, whose value is variable is defined as Region II. The boundary to separate Regions I and II can be detected through the constant value in thickness using our in-house code made in the MATLAB, which is marked in **Figure 7(a)**. And it is depicted that the Region I under 298 K is almost the same as that under 433 K. A similar observation can be seen in **Figure 7(b)**, although difference can be seen in $H_{-2.5}$, as $H_{-2.5}$ under 433 K evaporates for a quite long time at 50 ms ASOI, leading to a sharp reduction. Regions I and II are presented in **Figure 7(b)** by using the same criterion. It is worth noting that Region I at 5 ms and 50 ms ASOI are similar as well.

Overall, the mechanisms of fuel film formation are illustrated in **Figure 9** by applying the divided Regions I and II as mentioned above.

Region I also can be named as primary impingement region. The spray impinges on the wall directly, leading to some fuel sticking on it to form the film.

Region II also can be named as secondary impingement region. After fuel spray impingement, most of the fuel splashes off it. The splashing droplets are re-deposited on the wall to form the film because of coalescence and air force.

During injection: When fuel is ejected from the nozzle, liquid fuel breaks up into ligaments and large droplets. Through the spray propagation, the ligaments and large droplets break up into small ones owing to the interaction between the liquid fuel and ambient gas. In the case of $T_{amb} = 298$ K, after the primary impacting, some liquid fuel deposits on the wall to form Region I, and other fuel splashes off the wall. However, the splashed droplets may collide and coalesce with others, causing a change in velocity. Finally, these droplets may redeposit on the wall to form Region II. Furthermore, under high temperature conditions, less fuel can be seen on Region II,

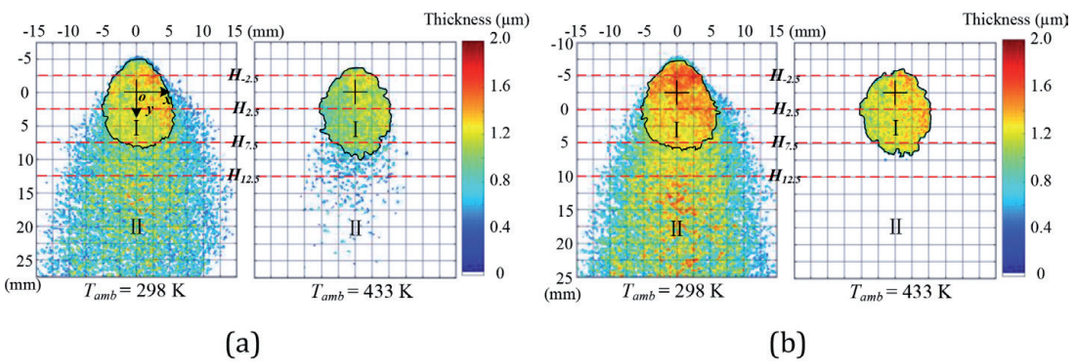

Figure 7.
Fuel film under different ambient temperatures. (a) 5 ms ASOI (b) 50 ms ASOI.

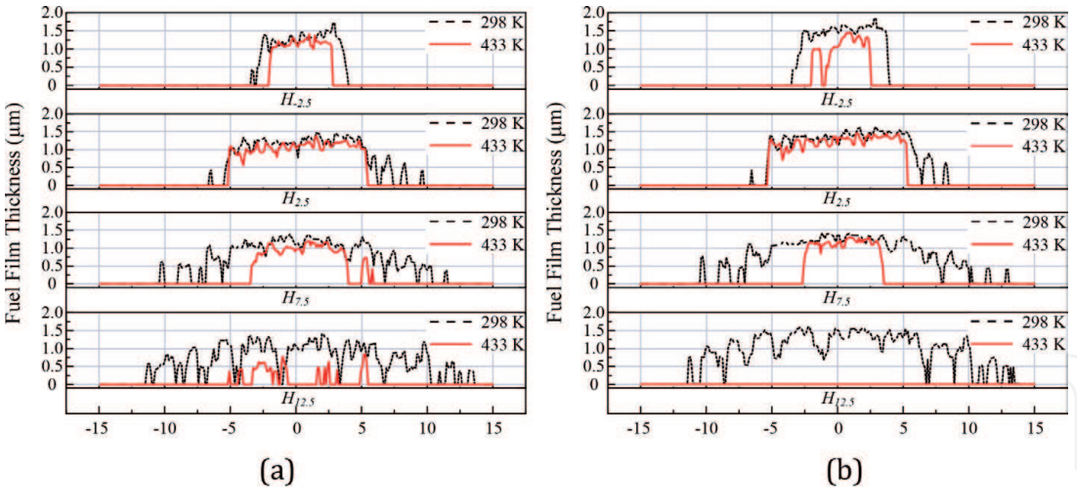

Figure 8.
Fuel film thickness along different lines. (a) 5 ms ASOI (b) 50 ms ASOI.

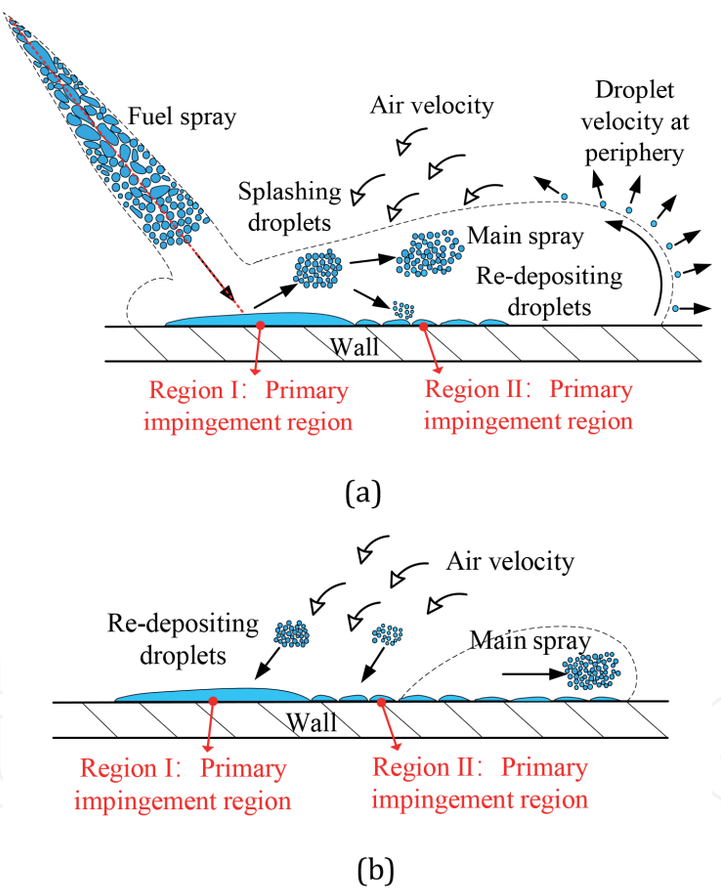

Figure 9.
Mechanisms of fuel film formation in different regions. (a) During injection. (b) After injection.

and the decreases in impinging droplets and fuel film evaporation should be the reasons for it.

After injection: Although no fuel spray can be seen, some tiny droplets are still in the air above the wall. Under T_{amb} = 298 K, the entrainment air changes the velocity of the splashing droplets. As a result, these droplets may re-impact on the wall to form Regions I and II. Under T_{amb} = 298 K, the same phenomena can be expected. But with considering the evaporation effect, the splashing droplets evaporate so quickly that few droplets can redeposit on the wall to from Region II. The fuel film

on Region I is mainly formed by the initial impingement, less effect can be seen on Region I, causing only periphery of film evaporating, which leads to fuel film on Region I almost the same as that under room temperature.

To summarize, the fuel film on Region I is caused by the direct impinging spray, affected less by the high ambient temperature. However, film on Region II is mainly caused by the redeposition of the splashing droplets. Under high temperature condition, the splashing droplets evaporate easily before reattaching the wall. Even some can redeposit to form film on the wall, it evaporates quickly due to the strong heat and mass transfer. As a result, fuel film on Region I is similar under T_{amb} = 298 K and 433 K, but varies greatly on Region II, as shown in **Figure 7**.

3.2 Effect of injection pressure

Figure 10 shows S under different injection pressures varying among 10, 20 and 30 MPa. Results at T_{amb} = 298 and 433 K are depicted by solid and open data. The horizontal axis represents time after start of fuel injection, and the vertical axis is S. The impingement distance is shown by dotted line. Owing to the fuel evaporation, S at T_{amb} = 433 K is slightly lower than that at T_{amb} = 298 K before impingement. Nevertheless, the difference becomes obvious after impingement, which can be attribute to the impingement facilitating fuel breakup and atomization. Moreover, larger difference in S can be found under P_{inj} = 10 MPa. And the longer time for spray propagation and evaporation may be one possible explanation for it. Although high injection promotes better atomization, the accelerated fuel spray shortens the spray development time, which might be another reason for explaining larger difference existing at low injection pressure.

H_i can be seen in **Figure 11**. The dotted line represents the end of injection (EOI) with the injection duration depicted. The impingement timing can be advanced under high injection pressure because of high momentum. At EOI, H_i at P_{inj} = 30 MPa is larger than that at 10 MPa under both evaporation and non-evaporation condition. The larger Weber number induced by high injection pressure results in more splashing droplets should be the reason for it. Although high injection pressure promotes better atomization, leading to fast evaporation of fuel, the stronger splashing phenomenon cannot be hindered. Furthermore, after EOI at T_{amb} = 433 K, as no fuel supply, H_i under P_{inj} = 30 MPa decreases more sharply

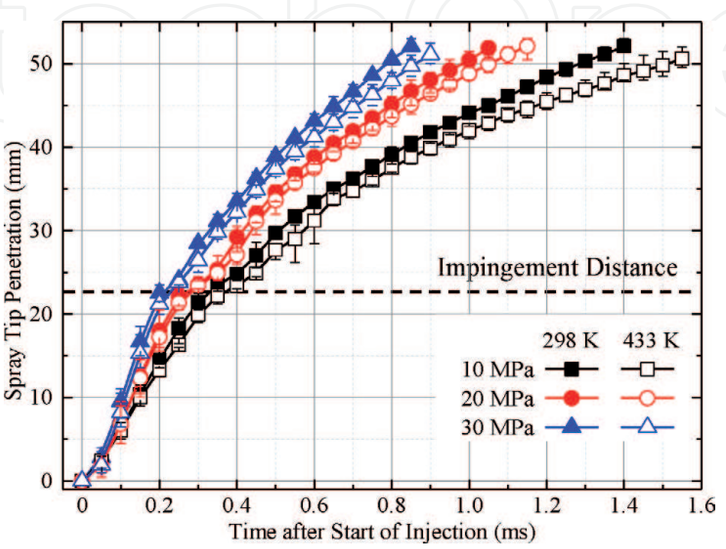

Figure 10.
Spray tip penetration under different injection pressures.

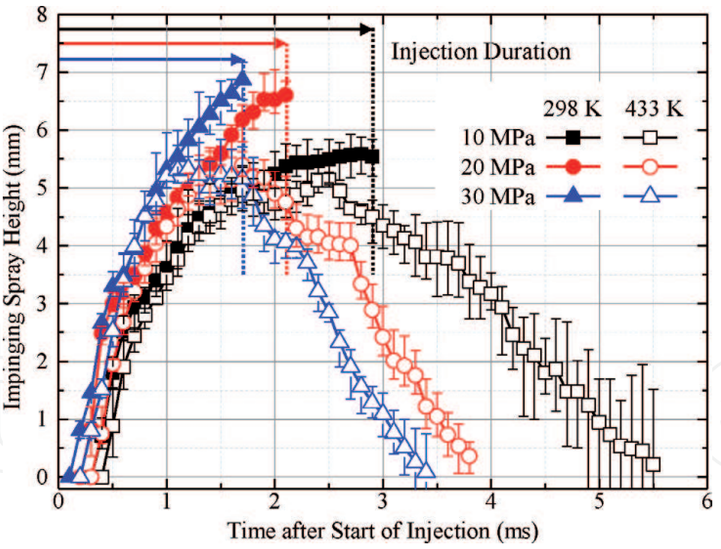

Figure 11.
Impinging spray height under different injection pressures.

than that under 10 MPa. And the better atomization and fast evaporation should be responsible for it.

In order to discuss the effect of injection pressure on the fuel film evolution, different timing at 5, 20, and 40 ms ASOI are selected to show at different injection pressures under T_{amb} = 298 K and 433 K, as shown **Figure 12**. The cross symbol is used to present the impingement point, and color bar is applied to show the thickness from 0 to 2.0 μm. It is important to see the maximum thickness is only 2 μm, and some reasons can be involved to explain it. Firstly, when liquid droplets impacting on the wall, various behaviors can be concluded such as "stick", "spread" and "splash", which are determined by the Weber number of the incident droplets [14]. Therefore, most droplets after impacting could splash off the wall, left few adhering on the wall. Secondly, the rough surface of the wall also promotes the droplets breakup and splashing of droplets after impingement [15]. Thirdly, the formed fuel film may be destroyed by incoming droplets and carried away by the air flow, leading to the maximum thickness at 2 μm. In addition, Ding et al. [16] and Maligne et al. [17] also obtained the similar observation.

Figure 12(a) shows fuel film evolution at different injection pressure from 10 to 30 MPa under T_{amb} = 298 K. It is clear to see that the film area increases with higher injection pressure. High injection pressure promotes better atomization, as a result, the splashing droplets may re-impact on the wall with the help of the air entrainment and vortex. Besides, the film on Region I decreases under high injection pressure. It was confirmed by Bai et al. [14, 18] that droplet behaviors change from "stick" to "splash" with lager Weber number. And high injection pressure accelerates velocity thus enlarging Weber number. As a result, more fuel splash off the wall after impingement, leading to less film on Region I. Moreover, the similar conclusion can be drawn from Mie scattering results in **Figures 10** and **11** that both S and H_i increase by elevated injection pressure because of droplets splashing. It should be noted that these splashing droplets may re-deposit on the wall to accumulate the film on Region II. Furthermore, film thickness increases with time on both regions as the secondary breakup droplets re-deposit, again.

Figure 12(b) shows fuel film evolution at different injection pressure from 10 to 30 MPa under T_{amb} = 433 K. Same as **Figure 12(a)**, film on Region I decrease with an increase in injection pressure as the splashing behaviors. Compared to T_{amb} = 298 K, fuel film on Region II decreases significantly owing to the fuel evaporation. Moreover, the thickness only becomes larger on Region I. The competition

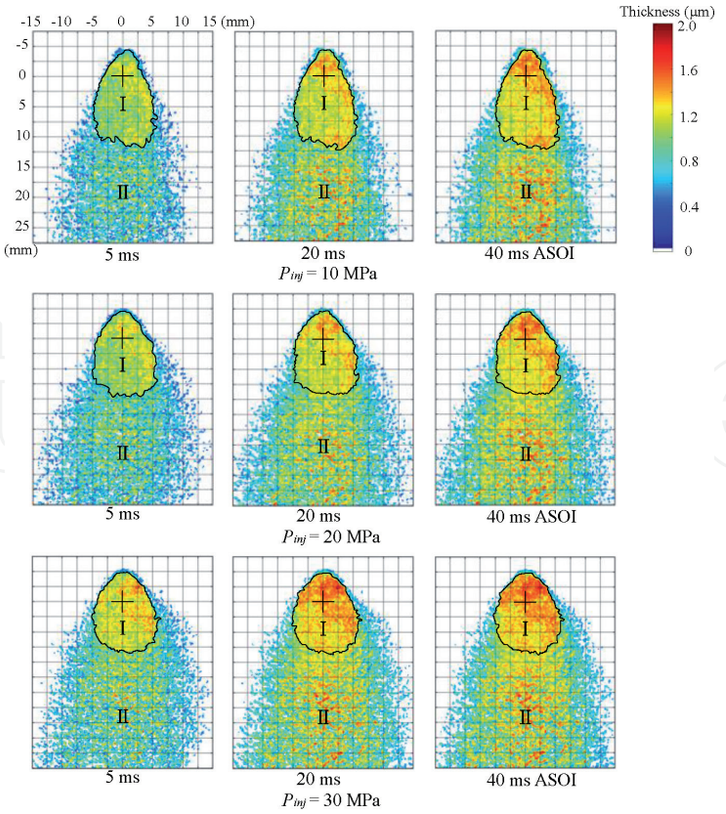

(a)

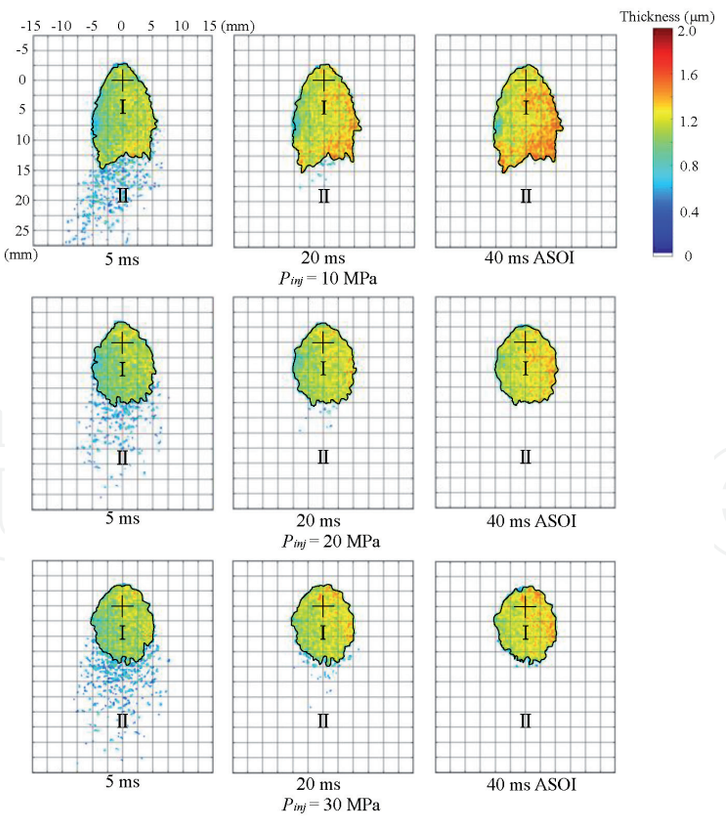

(b)

Figure 12.
Fuel film on the wall. (a) T_{amb} = 298 K. (b) T_{amb} = 433 K.

between droplets depositing and evaporation can be purposed. Maligne et al. [17] observed that film evaporates from thin to thick part due to heat transfer. Under high ambient temperature, the tiny droplets evaporate already before impacting.

Even the secondary droplets re-deposit on Region II to form film, it evaporates very quickly, thus only droplets accumulated on Region I can be observed owing to less heat transfer.

Figure 13 shows the fuel film mass with time after start of injection. The left vertical axis represents film mass, and right one represents the ratio of film mass to injection mass. The results under T_{amb} = 298 K and 433 K are depicted by solid and open data. As we known, two processed that spray development and fuel film formation can be summarized during spray wall interaction [19]. As the strong splashing phenomenon (see from the results of S and H_i above), the maximum only 13% of fuel adheres on the wall under T_{amb} = 298 K. Besides, it provides that film mass increases gradually with time due to the splashing droplets depositing on the wall under T_{amb} = 298 K. However, under T_{amb} = 433 K, the film mass only at P_{inj} = 10 MPa increases slightly with time. The transition changing from "splash" to "stick" tends to be responsible for it. More fuel adheres on Region I after impingement at lower injection pressure, leading to thick film. The splashing droplets re-deposit on Region I, it is difficult to evaporate as thick film existing, thus increasing mass slightly with time. For mass at P_{inj} = 20 and 30 MPa, the initial film mass on Region I is less in contrast to P_{inj} = 10 MPa. Even if the better breakup droplets re-arrive on the wall to form film, it evaporates immediately, which results in a slight decrease of mass. It is interesting to find that high injection pressure increases film mass under T_{amb} = 298 K but decreases film mass under T_{amb} = 433 K. And the opposite phenomena can be explained by different effect of injection pressure on fuel film formation under evaporation and non-evaporation conditions. Under T_{amb} = 298 K, the better atomized droplets accumulate on the wall easily including the first and second adhering on the wall, thus increasing mass at a high injection pressure. However, under T_{amb} = 433 K, the better atomized droplets evaporate easily before impacting on the wall for both incident and re-depositing droplets, leading to few film lefts. Besides, high-speed airflow also facilitates the film evaporation on the wall to decrease it.

Figure 14 describes the film area, and solid and open data are presented to show the results under T_{amb} = 298 K and 433 K, respectively. Similar to mass, film area increases with high injection pressure under T_{amb} = 298 K, but it decreases under T_{amb} = 433 K, which can be attribute to the different effects of injection pressure under ambient temperature conditions. More importantly, as the film evaporates from thin to thick, film area decreases with time, which is different to mass under P_{inj} = 10 MPa.

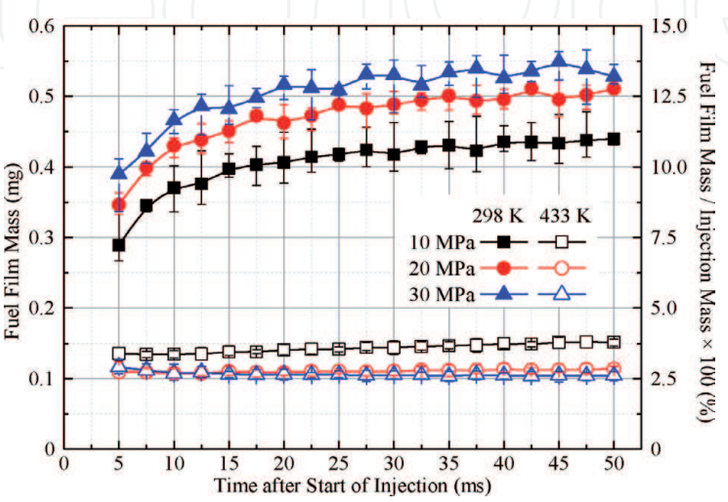

Figure 13.
Fuel film mass under different injection pressures.

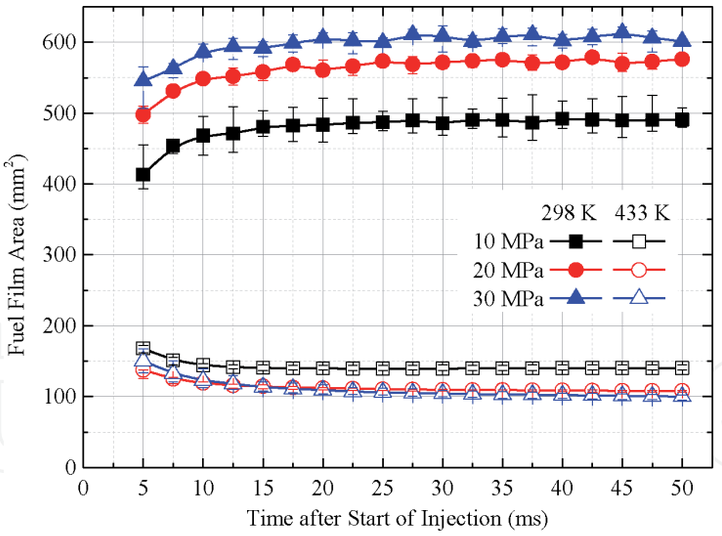

Figure 14.
Fuel film area under different injection pressures.

The film mass distribution at the thickness was defined for deeply study. As illustrated in **Figure 15**, fuel film thickness is presented as the horizontal axis, and film mass is shown by vertical axis. The film mass is calculated by each pixel as shown in the equation below:

$$M(h) = \sum_{i=0}^{\infty} h(i) \tag{1}$$

where the sum of fuel film mass in the thickness fraction between h ± 0.5 Δ h and h is defined as $M(h)$, and Δ h is 0.05 μm.

Figure 15 shows the film mass along thickness under different conditions at 40 ms ASOI. The peak value decreases dramatically, and curve becomes short owing to the evaporation effect when comparing the results of T_{amb} = 298 K and 433 K. It shows that mass under T_{amb} = 433 K at the thickness from 0.1–0.8 μm decreases to almost 0 in contrast to that under T_{amb} = 298 K, which can be the evidence that high temperature contributes more effort on the thin film evaporation than thick one, thus improving the film uniformity as the narrow shape under T_{amb} = 433 K, which is consistent of the observation in **Figure 12**. Besides, the role of injection pressure can be explained more by checking the smallest peak value at P_{inj} = 10 MPa under T_{amb} = 298 K, but the largest ones under T_{amb} = 433 K.

For better understanding the uniformity of the fuel film, the probability of mass should be used, and it must satisfy the normalization conditions:

$$\sum_{i=0}^{\infty} f_M(h_i) = 1 \tag{2}$$

where the $f_M(h)$ is the probability of $M(h)$.

As illustrated in **Figure 16**, the peak value of probability under T_{amb} = 433 K is much larger than that of T_{amb} = 298 K, indicating more uniform film formed on the wall. No thin film at the periphery should be the reason for it due to evaporation. It is interesting to find that under T_{amb} = 433 K, although peak value of mass occurs at P_{inj} = 10 MPa, but the probability at P_{inj} = 30 MPa becomes the largest one, suggesting high injection promotes film uniformity under evaporation condition. However, under non evaporation condition, less influence of injection pressure can be detected.

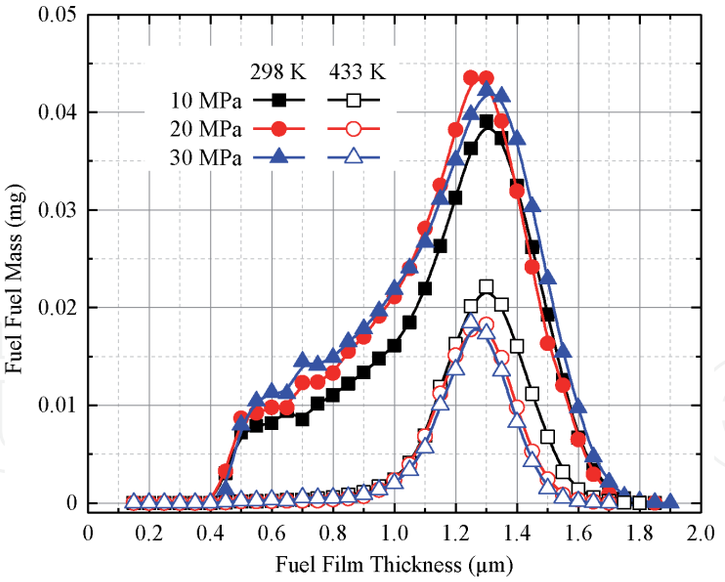

Figure 15.
Fuel film mass distribution under different injection pressures.

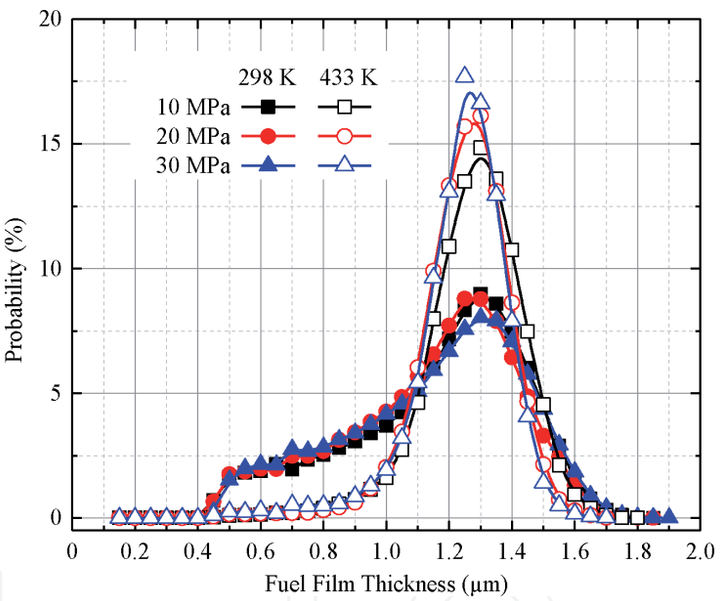

Figure 16.
Probability of film thickness under different injection pressures.

3.3 Effect of ambient pressure

Figure 17 shows the S under different ambient pressures, with results of T_{amb} = 298 and 433 K depicted by solid and open symbols. It suggests that the increased ambient pressure decreases S, and the raised density of the air results in stronger air-fuel entrainment and less spray momentum should be the reason for that under both non-evaporation and evaporation conditions. H_i under different conditions are compared in **Figure 18**. At the initial stage from 0.2 to 1.0 ms ASOI, H_i is larger under low ambient pressure. H_i generates easily as less resistance from ambient pressure should be the reason for it. While, H_i becomes larger under high ambient pressure with spray development. The raised ambient gas density from high ambient pressure results in strong air-fuel entrainment. Therefore, more air-fuel mixture can be expected after impingement, thus increasing H_i under high ambient pressure. In contrast to that, after EOI, the spray propagates along the wall

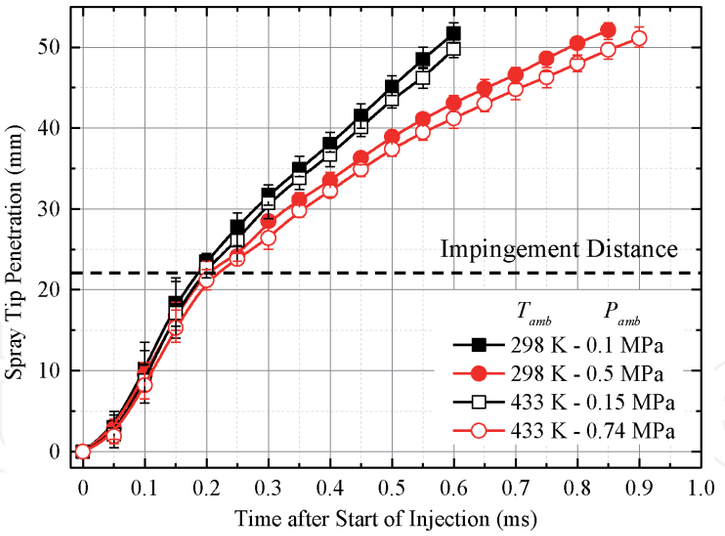

Figure 17.
Spray tip penetration under different ambient pressures.

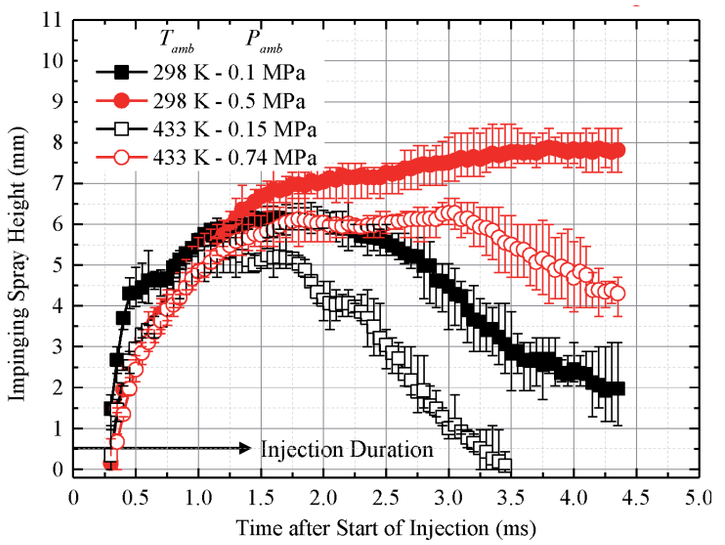

Figure 18.
Impinging spray height under different ambient pressures.

quickly with less air drag force under low ambient pressure, leading to no fuel supply. Therefore, H_i decrease sharply after EOI. Besides, the high ambient temperate promotes this behavior. However, owing to the slow air-fuel movement under high ambient pressure, H_i can keeps constant and even increases to some extent after EOI, suggesting high ambient pressure enlarges H_i. One thing should be noted that although the high ambient pressure suppresses H_i, the behaviors of slow movement accumulating H_i cannot be hindered.

In order to discuss the effect of ambient pressure on the fuel film evolution, different timing at 5, 20, and 40 ms ASOI are selected to show at ambient pressures under T_{amb} = 298 K and 433 K, as shown **Figure 19**. The cross symbol is used to present the impingement point, and color bar is applied to show the thickness from 0 to 2.0 μm. It has already illustrated in **Figure 9** that two regions on the fuel film on the wall could be separated with different formation mechanism as Regions I and II. And the ambient pressure has more influences on the film formation on Region II.

Figure 19(a) illustrates that fuel film on both Regions I and II increases with time elapse, and the re-depositing droplets accumulating on the wall should be

the reason for it. Moreover, it has to be noted that the film area increases with high ambient pressure. Three main reasons can be summarized. Firstly, elevated ambient pressure promotes better atomization, and these atomized droplets re-arrive on the wall easily by vortex to increase film. Secondly, high ambient pressure decelerates fuel spray before impingement, leading to decreasing Weber number. Therefore, the droplet behaviors may change from "splash" to "spread" or "stick" with small Weber number, causing adhered film increase. Thirdly, under high ambient pressure, the splashing droplets could collide and coalesce with others easily, and finally re-deposit on the wall to increase the fuel film.

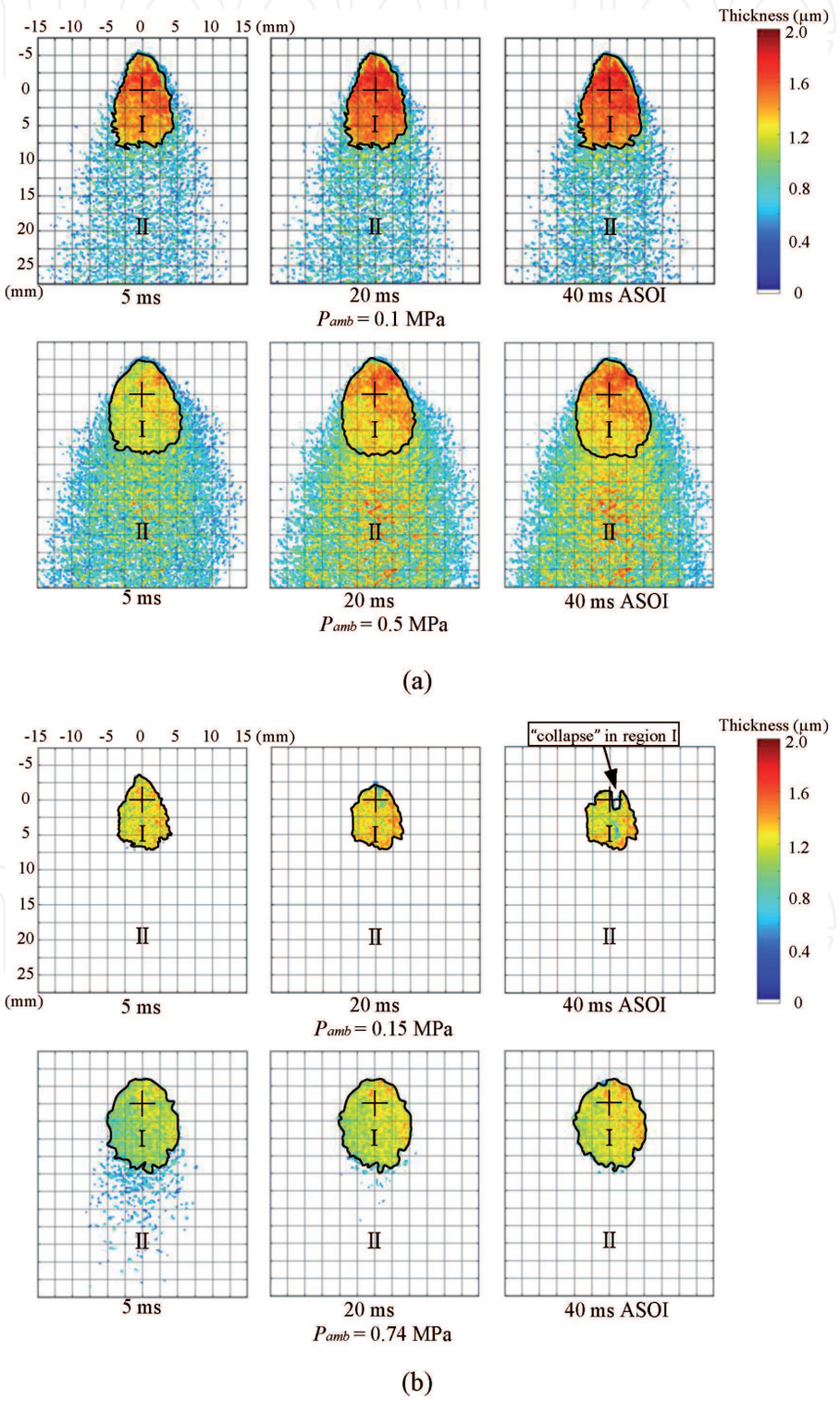

Figure 19.
Evolution of fuel film on the wall. (a) T_{amb} = 298 K. (b) T_{amb} = 433 K.

Figure 19(b) illustrates the fuel film evolution on the wall at T_{amb} = 433 K. It is clear that owing to evaporation, fuel film area decreases obviously with time. Furthermore, more fuel locates on Region I other than Region II, and the less heat transfer at thick film should be the reason for it. Under T_{amb} = 433 K, some of the splashing droplets evaporate before re-impacting on the wall. And the survived re-depositing droplets on Region II evaporate immediately as strong hear transfer, leading to more fuel film accumulating on Region II at last. While, the survived ones impact on Region I then form film on it successfully. It can be seen that fuel film exist on Region II at 5 ms ASOI under P_{amb} = 0.74 MPa, and the large droplets re-depositing and adhering on the wall before evaporation should be the main reason for it. Besides, the fuel film area under P_{amb} = 0.74 MPa is larger than that under P_{amb} = 0.15 MPa. In addition to the reasons discussed above, high ambient pressure hinders the film evaporation to a certain extent could be another reason. One more interesting thing is that under P_{amb} = 0.15 MPa, fuel film evaporates from periphery until 40 ms ASOI, and the "collapse" appearing in the film affects the film uniformity, which will be discussed more in the following part.

Figure 20 shows the fuel film mass with time after start of injection. The left vertical axis represents film mass, and right one represents the ratio of film mass to injection mass. The results under T_{amb} = 298 K and 433 K are depicted by solid and open data. It depicts that film mass increases with time gradually under T_{amb} = 298 K. And the re-depositing droplets after splashing should be responsible for it. Noticed that the increased amplitude of film mass under P_{amb} = 0.5 MPa is much larger when compared to of P_{amb} = 0.1 MPa. On one hand, high ambient pressure enlarges and decelerate droplets, leading to more droplets tend to re-deposit on the wall. On the other hand, the behavior transition from "splash" to "stich" increases film on the wall. But looking at the mass under T_{amb} = 433 K, it decreases with time slightly due to evaporation. Even if some re-deposited droplets adhere on the wall, the evaporation effect cannot be ignored. More importantly, mass under P_{amb} = 0.74 MPa is larger than that under P_{amb} = 0.15 MPa. As explained in the experimental condition, T_{sat} (398 K) < T_{amb} under P_{amb} = 0.15 MPa, indicating a strong film evaporation. While, T_{sat} (472 K) is larger than T_{amb} under P_{amb} = 0.74 MPa, and a slow evaporation can be expected. Recently, Schulz et al. [20] found that the time for film evaporation duration increases at elevated ambient pressure, implying that high

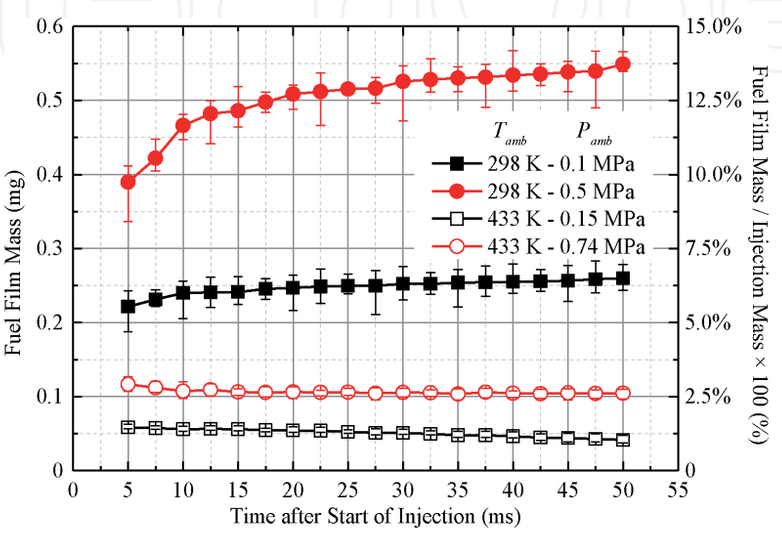

Figure 20.
Fuel film mass under different ambient pressures.

ambient pressure has a significant effect on inhibiting evaporation of fuel film. This founding is confirmed by Kim et al. [21] from their single droplet experiment and Tao et al. [22] from the computational fluid dynamics (CFD)results. Furthermore, the results that film mass under P_{amb} = 0.74 MPa is larger than that under P_{amb} = 0.15 MPa can also demonstrate that high ambient pressure inhibits the fuel evaporation.

Figure 21 describes the film area, and solid and open data are presented to show the results under T_{amb} = 298 K and 433 K, respectively. As the re-depositing droplets impact on the same location, leading to large increase in mass but little increase in area. Therefore, fuel film under T_{amb} = 298 K increases with time slightly. Same as film mass, the area increases with high ambient pressure. Under non-evaporation condition, the large size, low velocity, "stick" behavior and easy re-deposition should be attribute to it. Under evaporation condition, in addition to the above factors, the inhibition of film evaporation under high ambient pressure should be another reason for it.

Figure 22 shows the film mass along thickness under different conditions at 40 ms ASOI. And the results under T_{amb} = 298 K and 433 K are shown by solid and

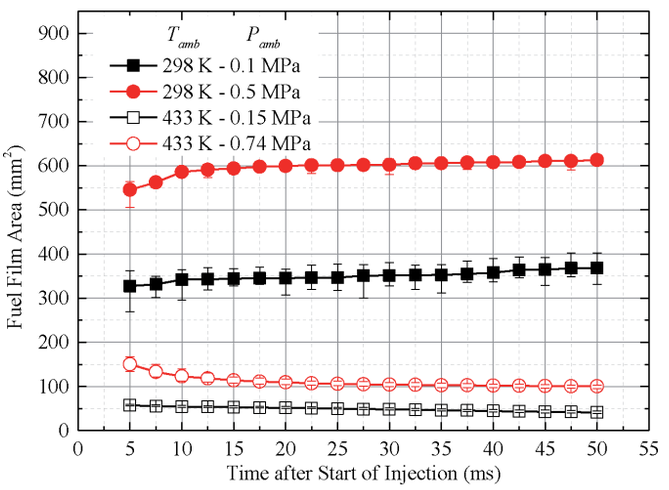

Figure 21.
Fuel film area under different ambient pressures.

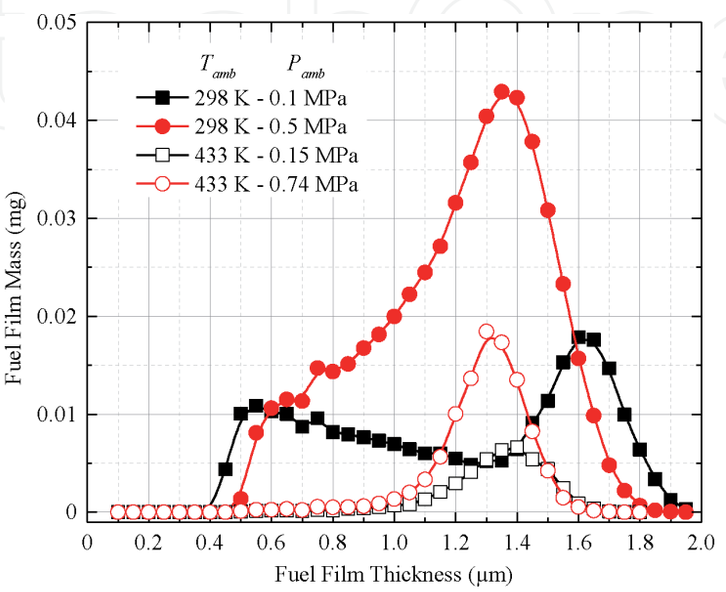

Figure 22.
Fuel film mass distribution under different ambient pressures.

open symbols, respectively. It reveals that the peak value increases significantly with high ambient pressure. It should be clarified that under T_{amb} = 298 K, tow peak values at 0.5 and 1.6 μm can be observed for P_{amb} = 0.1 MPa condition, indicating film accumulated on Region II and the central of region I. However, by increasing the ambient pressure to 0.5 MPa, it is interesting to find these two peaks merge into one, indicating more uniform film form under high ambient pressure.

Figure 23 shows the probability of film mass along thickness under different conditions at 40 ms ASOI, and the results under T_{amb} = 298 K and 433 K are depicted by solid and open symbols, respectively. The probability increases sharply under evaporation condition, indicating high temperature facilitates uniform film on the wall. And the evaporation occurs from thin to thick should be the main reason. Special attention should be taken that not only ambient temperature, but also ambient pressure can improve the fuel film uniformity. Elevating the ambient pressure at a certain temperature can increase the density of the ambient gas, leading to a strong interaction between air gas and fuel. As a result, fuel spray angle increases, and droplets kinetic energy decreases. Eventually, the droplets attach o more evenly on the wall, thereby forming a uniform film on the wall. Because of this reason, under T_{amb} = 298 K, when ambient pressure increased from 0.1 to 0.5 MPa, these two peaks merge into one, indicating large improvement for film uniformity. Similarly, under T_{amb} = 433 K, as less film located on Region II, the two peaks disappear. By increasing the ambient pressure from 0.15 to 0.74 MPa, peak value increases, suggesting uniformity improved, although not so obvious as that under non-evaporation condition.

To sum up, **Figure 24** displays the relationship between the saturation vapor pressure curve and the tested conditions. It shows that above the curve toluene is under the liquid phase but transits to vapor phase below the curve. By increasing the ambient pressure from 0.1 to 0.5 MPa under T_{amb} = 298 K, the ambient density increases. Then, the stronger entrainment and air resistance can be expected, leading to low velocity and large size of the droplets, and behavior changing from "splash" to "stick", which are the reasons for fuel film increase. In addition, increased the ambient pressure from 0.15 to 0.74 MPa under T_{amb} = 433 K, because of the transient from vapor to liquid phase, the decrease in evaporation rate as one more reason increases fuel film on the wall.

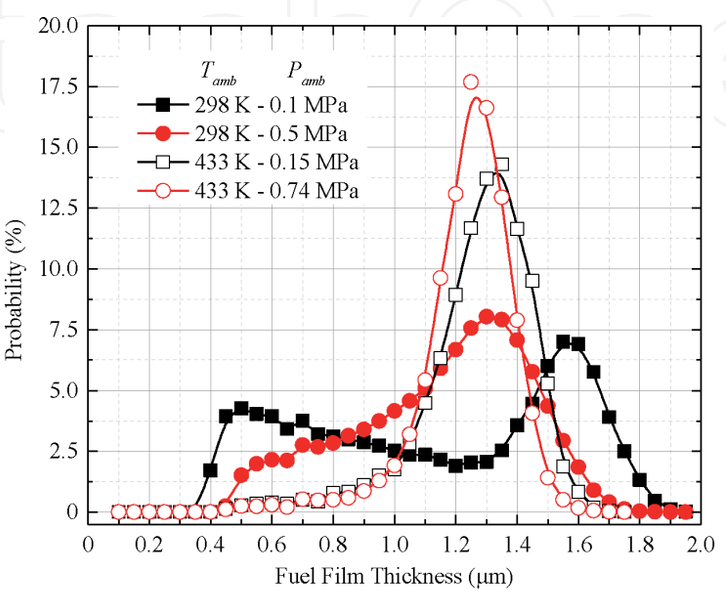

Figure 23.
Probability of film thickness under different ambient pressures.

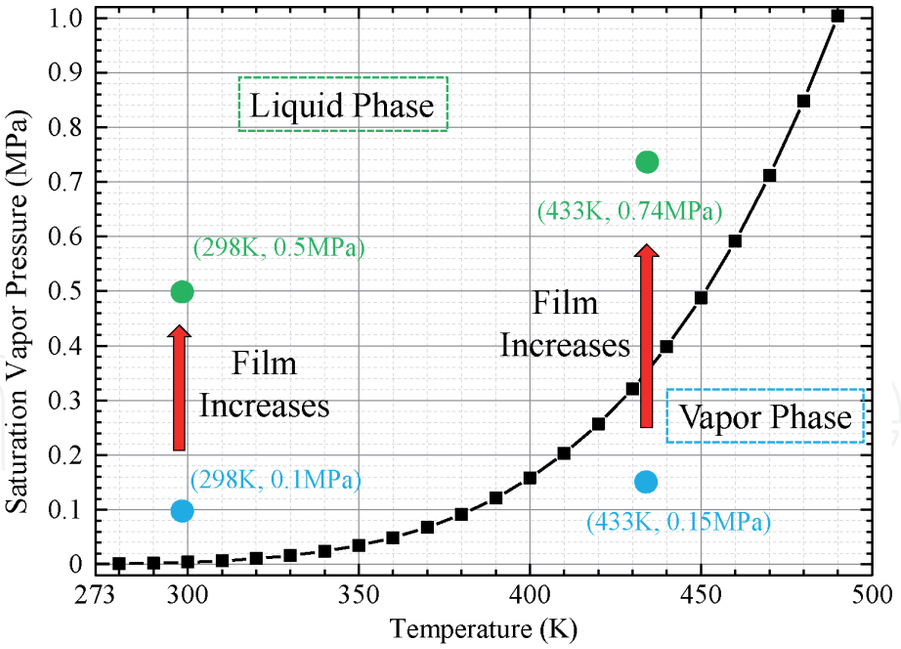

Figure 24.
Saturation vapor curve of tested fuel.

3.4 Fuel film evaporation characteristics

Figure 25(a) shows the fuel film evolution at P_{amb} = 0.15 MPa. Different timings at 50, 70, 100, and 150 ms ASOI are selected to depict and the color bar presents thickness from 0 to 2.0 μm with cross symbol being as impingement point (o). Owing to the fuel evaporation, the film area decreases with time. Furthermore, the film evaporates from the cross symbol to downstream, making the fuel film "moves downward". The film thickness increases from up to downstream due to the interaction of fuel spray and wall, leading to the fuel film evaporates quickly at the impingement region. As a result, it appears the film moving downward. Besides, the increased injection pressure decreases film area significantly. Three reasons can be concluded. Firstly, the high injection promotes better atomization, resulting in more tiny droplets evaporate before impacting on the wall. Secondly, even if some droplets survive to impact on the wall, with larger Weber number, the trend of "splash" after impingement can be expected. Thirdly, even though fuel finally sticks on the wall, the air flow with high velocity improves the evaporation rate, leading to less film left. Noteworthy is that the film evaporates from the periphery to the central of film firstly as Maligne and Bruneaux [17] reported, then evaporates from the central causing a "hollow" in the film, which will be analyzed in the following part. It is interesting that under the elevated injection pressure, more film can be observed near the cross symbol, especially at 150 ms ASOI. The increased injection pressure enlarges Weber number, leading to more fuel "splash" instead of "spread". Finally, less fuel accumulates at the downstream.

Figure 25(b) shows the fuel film evolution at P_{amb} = 0.74 MPa. More fuel film can be seen left on the wall when ambient pressure increased to 0.74 MPa. The same as **Figure 25(a)**, it is evident that fuel film area decreases sharply against high injection pressure. In addition, the increased ambient pressure also increases film area. The droplets are decelerated by stronger air force of high ambient pressure. Therefore, more droplets tend to "stick" on the wall, resulting in more film formed. Besides, even some droplets splash off the wall, the splashing droplets tend to collide and then coalesce with others. Finally, these larger droplets redeposit on the wall more easily, thus accumulating more film. Moreover, the evaporation rate decreases under high ambient pressure, leading to more film left. And more discussions about the evaporation rate

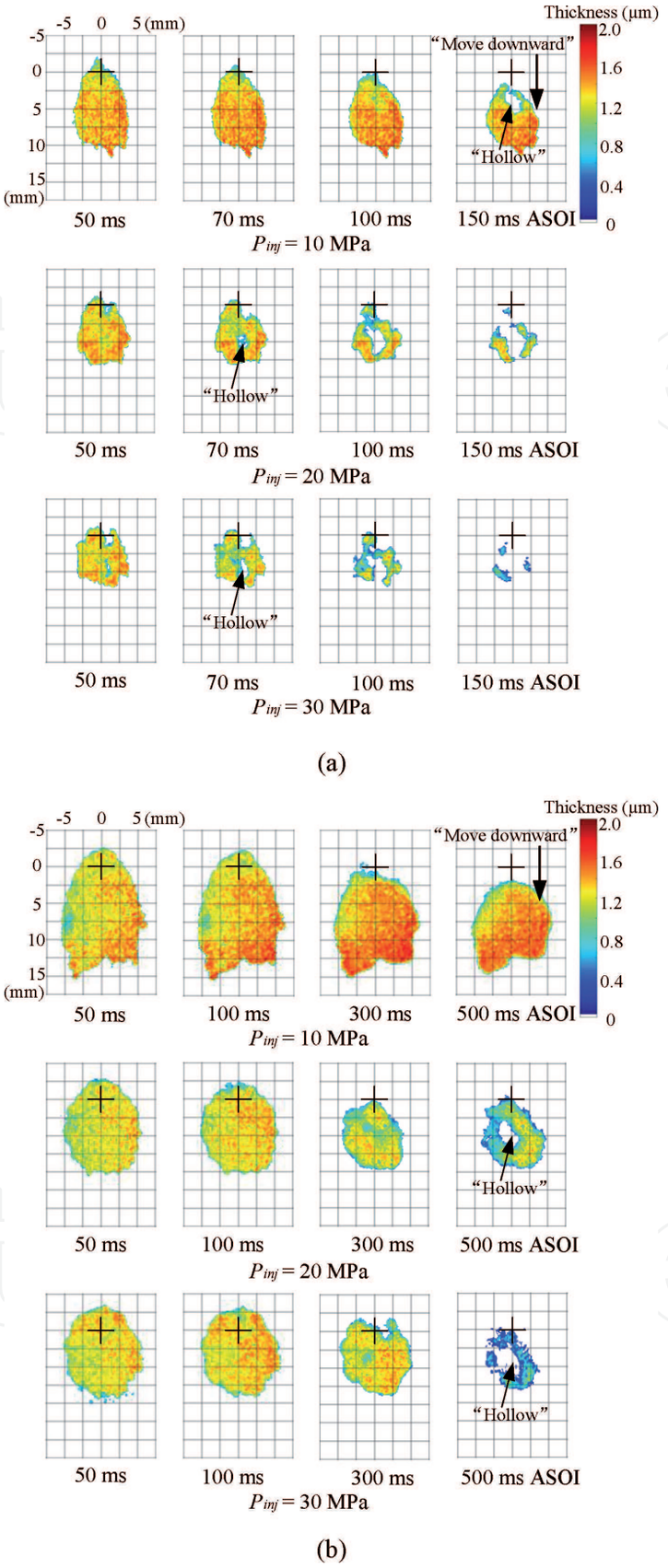

Figure 25.
Evolution of fuel film. (a) P_{amb} = 0.15 MPa. (b) P_{amb} = 0.74 MPa.

will be discussed in the next part. Besides, similar to **Figure 25(a)**, more fuel can be seen near the cross symbol with an increase in injection pressure at 500 ms ASOI.

Figure 26 shows fuel film mass under different conditions with left vertical axis being mass and right one being the ratio of film mass to injection mass. Results

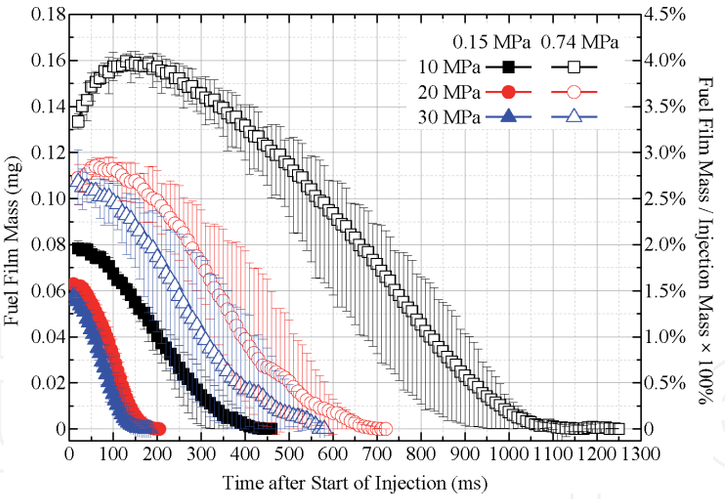

Figure 26.
Evaporation characteristics of fuel film mass.

under P_{amb} = 0.15 and 0.74 MPa are shown by filled and open data. It is evident that the mass increases with an increase in injection pressure due to the better atomization and fast evaporating rate. While, the mass increases with an increase in ambient pressure. More fuel sticking on the wall and low evaporating rate should be responsible for it. It should be noted that the film mass firstly increases and then decreases under only one case of P_{inj} = 10 MPa, P_{amb} = 0.74 MPa. Although the injection duration is only 2.9 ms, mass increases until 200 ms ASOI. It should be attributed to the lowest velocity of liquid droplets and largest size of them. As described above, under high ambient but low injection pressures condition, the spray is decelerated causing the impacting droplets arrive at the wall relatively late, which is the main reason for mass increasing gradually. Moreover, droplets tend to coalesce into larger more after impingement making it difficult to evaporate. In addition, droplets re-deposit on the wall easily under this case. It is interesting to see that the maximum ratio is approximately 4%, while the minimum one is 1.5%, suggesting most fuel evaporates or splashes off the wall.

Figure 27 shows fuel film area under different conditions. Results under P_{amb} = 0.15 and 0.74 MPa are shown by filled and open data. Similar to mass, the elevated injection pressure enlarges film area decreases but ambient pressure increases it with the same reason as mass. More importantly, different to mass, no obvious increase in area can be seen under P_{inj} = 10 MPa, P_{amb} = 0.74 MPa, implying that the impacting droplets arrive at the same location, leading to only mass increase. Besides, the lifetime of fuel film can be obtained from **Figures 26** and **27**, which will be discussed more in **Figure 28**.

Figure 29 provides the details about the "hollow" development in fuel film under P_{inj} = 10 MPa, P_{amb} = 0.15 MPa. It reveals that film evaporates at periphery from 60 to 120 ms ASOI, causing it "moving downward" as analyzed in **Figure 25**. Generally, evaporation occurs during the film formation, also leading to the film becomes thin with time for the whole region. At around 140 ms, it shows "hollow" occurs. With "hollow" development, film becomes less uniform, leading to quick evaporation at "hollow" until all evaporated.

A conceptual model for fuel film evaporation is proposed here to describe its mechanism and evaporation dynamic, as shown in **Figure 30**. Three processed can be summarized "Evaporate from periphery - Hollow occur - Evaporate from hollow". Because the fuel film at the periphery is relatively thin, strong evaporation can be expected owing to heat transfer in contrast to central part. With the consideration of the flat wall used with roughness, the film is non-uniform initially. Then,

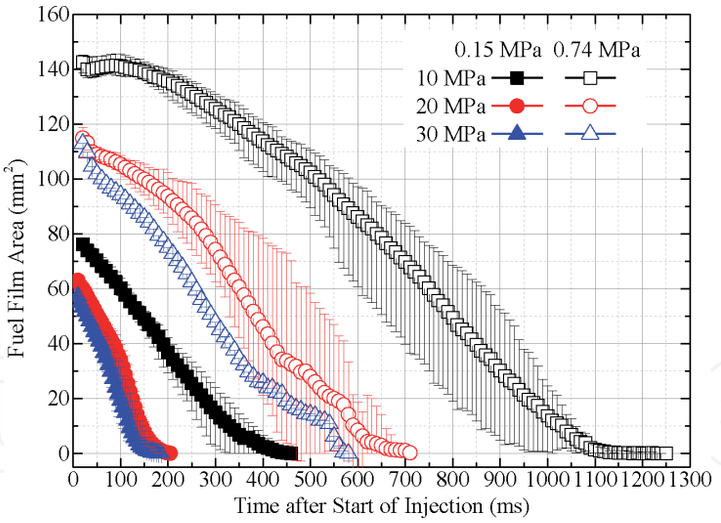

Figure 27.
Evaporation characteristics of fuel film area.

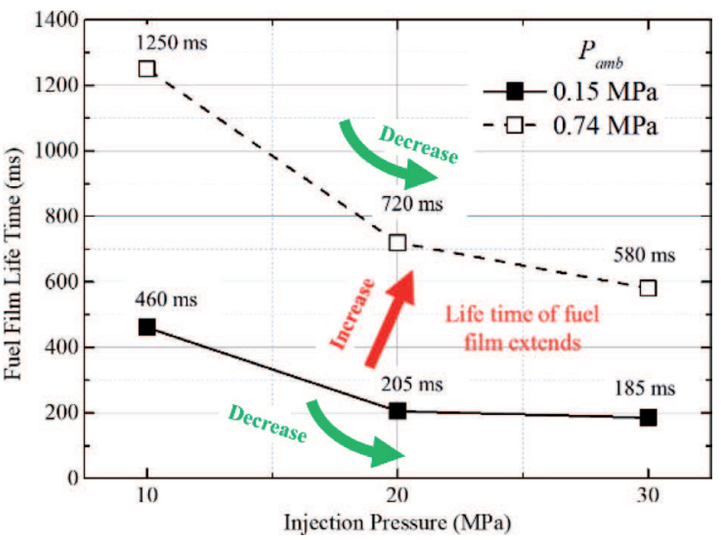

Figure 28.
Fuel film lifetime.

"hollow" appears in the film with evaporation, leading to film "breakup". With the "hollow" development, film evaporation is facilitated, and film becomes less uniform until all evaporates finally.

Figure 28 illustrates the fuel film lifetime under different conditions. Noting that the lifetime is calculated from the start of injection until all film evaporates, as shown in **Figures 26** and **27**. One more thing should be noted that although the lifetime is quite longer than one cycle of the real working condition in gasoline engine, lifetime is an important factor to evaluate film evaporation characteristics, especially for validating the simulation result. The observation shows that injection pressure decreases film lifetime owing to the enhanced evaporation rate and better atomization. Moreover, the decreased lifetime from 10 to 20 MPa is more obvious than that from 20 to 30 MPa, suggesting limitation may exist for the high injection pressure shortening lifetime. But ambient pressure increases the lifetime mainly due to the liquid/vapor transition by elevating ambient pressure from 0.15 to 0.74 MPa. The phase transition can decrease the evaporation rate sharply, leading to longer lifetime of the film. Besides, this may be another reason for the mass increases with high ambient pressure. But no influence can be found from the injection pressure on phase changing.

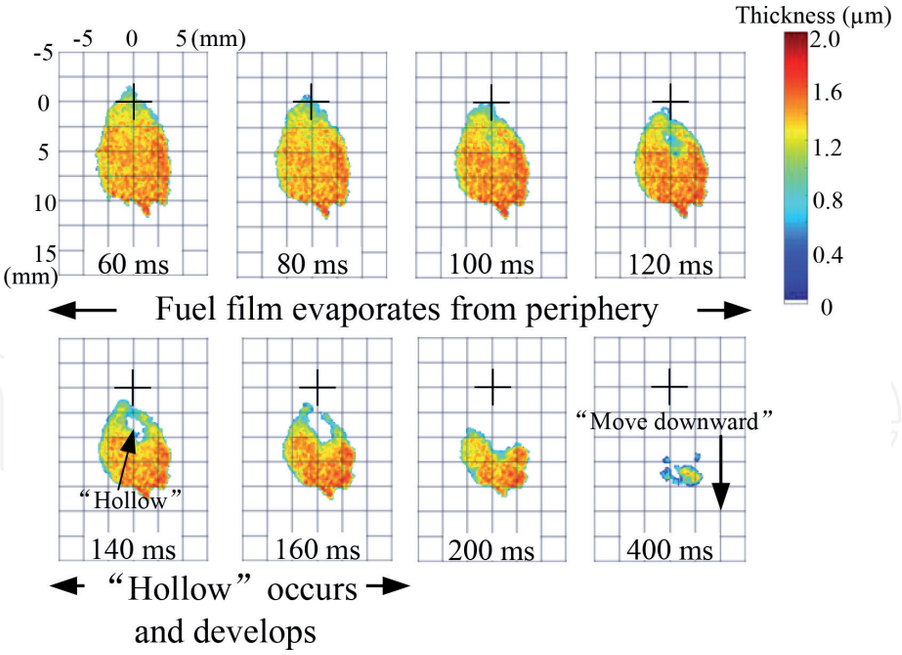

Figure 29.
"Hollow" development.

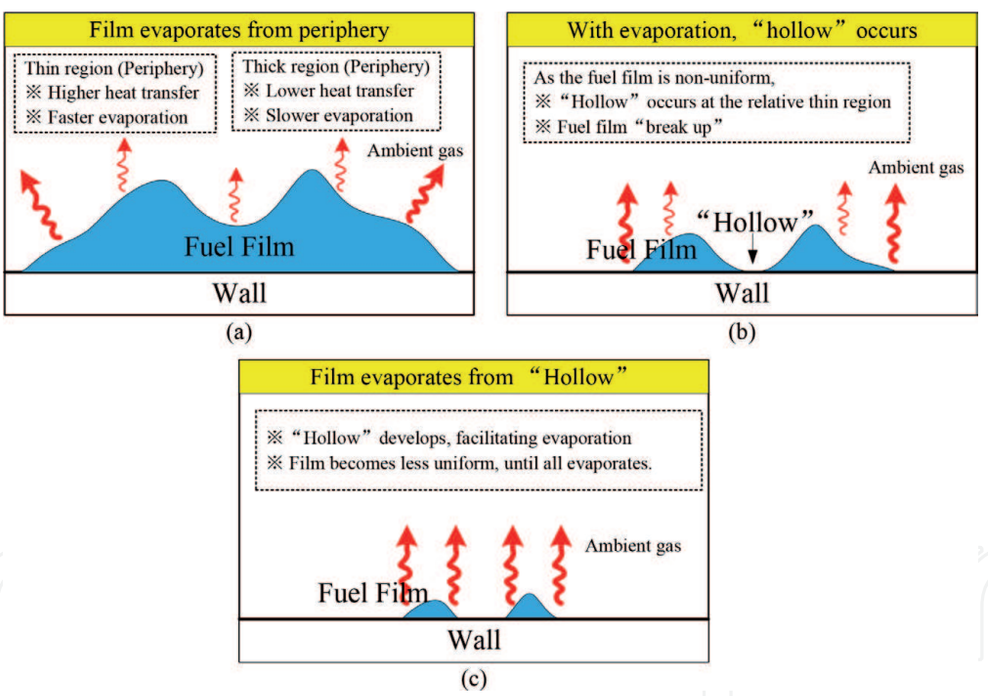

Figure 30.
Schematic conceptual model. (a) Film evaporates from periphery. (b) With evaporation, "hollow"occurs. (c) Film evaporates from "hollow".

4. Conclusions

This chapter discussed about the fuel spray and impingement under non-evaporation and evaporation conditions. The impinging spray development and fuel film formation as well as evaporation characteristics were checked and compared, the major conclusions are summarized as follows:

1. Different impingement regions were characterized through the formation of fuel film, known as the primary impingement region (called Region I) and the

secondary impingement region (called Region II). Furthermore, high ambient temperature exerts more influence on the fuel film formation for the Region II.

2. During the injection, a high injection pressure accelerates the fuel spray and favors the atomization of fuel, thus enlarging S and H_i of liquid phase under both T_{amb} = 298 K and T_{amb} = 433 K. Under T_{amb} = 298 K, injection pressure increases the fuel film mass and area. However, under T_{amb} = 433 K, injection pressure decreases the them, and the better atomization and easy evaporation of the fuel are the main reasons for it.

3. The increased ambient pressure increases the density of the gas, resulting in strong air-fuel entertainment and less momentum, thus shortening S and increasing H_i. Moreover, higher ambient pressure increases the fuel film mass and area under both T_{amb} = 298 K and T_{amb} = 433 K.

4. The fuel film firstly evaporates from periphery, leading to fuel film "moving downward". Then, "hollow" occurs and develops, resulting in less uniformity of fuel film. Finally, the fuel film evaporates from the "hollow" until all evaporated. The fuel film lifetime is shortened by increasing injection pressure, but it extends with an increase in ambient pressure.

Acknowledgements

The author would like to acknowledge National Natural Science Foundation of China [51909037] and State Key Laboratory of Clean Energy Utilization [ZJU-CEU 2019005].

Nomenclature

CFD	Computational fluid dynamics
DISI	Direct injection spark ignition
RIM	Refractive index matching
PFI	Port fuel injection
UHC	Unburned hydrocarbon
PM	Particulate matter
PN	Particle number
EV	Electric vehicle
T_{sat}	Saturated temperatures
fps	Frames per second
S	Spray tip penetration
H_i	Impinging spray height
L_w	Distance to wall
L_r	Radial distance
ASOI	After start of injection
EOI	End of injection
T_{amb}	Ambient temperature
P_{inj}	Injection pressure
P_{amb}	Ambient pressure

IntechOpen

IntechOpen

Author details

Hongliang Luo
Hiroshima University, Higashi-Hiroshima, Japan Foshan University, Foshan, P.R. China

*Address all correspondence to: luo@hiroshima-u.ac.jp

IntechOpen

© 2021 The Author(s). Licensee IntechOpen. This chapter is distributed under the terms of the Creative Commons Attribution License (http://creativecommons.org/licenses/by/3.0), which permits unrestricted use, distribution, and reproduction in any medium, provided the original work is properly cited. CC BY

References

[1] Maly RR. State of the art and future needs in SI engine combustion. Symposium (International) on Combustion 1994; 25(1): 111-124. https://doi.org/10.1016/S0082-0784(06)80635-1

[2] Drake MC and Haworth DC. Advanced gasoline engine development using optical diagnostics and numerical modeling. Proceedings of the Combustion Institute 2007; 31(1): 99-124. https://doi.org/10.1016/j.proci.2006.08.120

[3] Kalantari D, Tropea C. Spray impact onto flat and rigid walls: Empirical characterization and modelling. International Journal of Multiphase Flow 2007; 33(5): 525-544. https://doi.org/10.1016/j.ijmultiphaseflow.2006.09.008

[4] Tanaka D, Uchida R, Noda T, Kolbeck A, Henkel S, Hardalupas Y, Taylor A, Aradi, A. Effects of fuel properties associated with in-cylinder behavior on particulate number from a direct injection gasoline engine. SAE Technical Paper, 2017-01-1002; 2017. https://doi.org/10.4271/2017-01-1002

[5] Zhao F, Lai MC, Harrington DL. Automotive spark-ignited direct-injection gasoline engines. Progress in energy and combustion science 1999; 25(5): 437-562. https://doi.org/10.1016/S0360-1285(99)00004-0

[6] Moreira ALN, Moita AS, & Panao MR. Advances and challenges in explaining fuel spray impingement: How much of single droplet impact research is useful?. Progress in energy and combustion science 2010; 36(5): 554-580. https://doi.org/10.1016/j.pecs.2010.01.002

[7] Park SW and Lee CS. Macroscopic and microscopic characteristics of a fuel spray impinged on the wall. Experiments in fluids 2004; 37 (5): 745-762. https://doi.org/10.1007/s00348-004-0866-3

[8] Andreassi L, Ubertini S, & Allocca L. Experimental and numerical analysis of high pressure diesel spray–wall interaction. International journal of multiphase flow 2007; 33(7): 742-765. https://doi.org/10.1016/j.ijmultiphaseflow.2007.01.003

[9] Guo M, Shimasaki N, Nishida K, Ogata Y, Wada Y. Experimental study on fuel spray characteristics under atmospheric and pressurized cross-flow conditions. Fuel 2016; 184:846-855. https://doi.org/10.1016/j.fuel.2016.07.083

[10] Luo H, Uchitomi S, Nishida K, Ogata Y, Zhang W, Fujikawa T. Experimental Investigation on Fuel Film Formation of Spray Impingement on Flat Walls with Different Surface Roughness. Atomization and Sprays, 2017; 27(7): 611-628. DOI: 10.1615/AtomizSpr.2017019706

[11] Luo H, Nishida K, Ogata Y. Evaporation characteristics of fuel adhesion on the wall after spray impingement under different conditions through RIM measurement system. Fuel, 2019;258: 116163. https://doi.org/10.1016/j.fuel.2019.116163

[12] Luo H, Nishida K, Uchitomi S, Ogata Y, Zhang W, Fujikawa T. Effect of Spray Impinging Distance on Piston Top Fuel Adhesion in Direct Injection Gasoline Engines. International Journal of Engine Research, 2020; 21(5):742-754. https://doi.org/10.1177/1468087418774175

[13] Luo H, Nishida K, Uchitomi S, Ogata Y, Zhang W, Fujikawa T. Effect of temperature on fuel adhesion under spray-wall impingement condition.

Fuel 2018, 234:56-65. https://doi.org/10.1016/j.fuel.2018.07.021

[14] Bai C, Gosman AD. Development of methodology for spray impingement simulation. J Engines 1995,104(3):550-68. https://www.jstor.org/stable/44633238

[15] Mundo CHR, Sommerfeld M, Tropea C. Droplet-wall collisions: experimental studies of the formation and breakup process. Int J Multiph Flow 1995;21(2):151-73.

[16] Ding CP, Sjöberg M, Vuilleumier D, Reuss DL, He X, Böhm B. Fuel film thickness measurements using refractive index matching in a stratified-charge SI engine operated on E30 and alkylate fuels. Exp Fluids 2018;59(3):59. https://doi.org/10.1007/s00348-018-2512-5

[17] Maligne D, Bruneaux G. Time-resolved fuel film thickness measurement for direct injection SI engines using refractive index matching. SAE Tech Paper 2011. 2011-01-1215. https://doi.org/10.4271/2011-01-1215

[18] Bai C, Rusche H, Gosman AD. Modeling of gasoline spray impingement. Atom Sprays 2002;12(1-3):1-27. DOI: 10.1615/AtomizSpr.v12.i123.10

[19] Baumgarten C. Mixture Formation in Internal Combustion Engines. Germany: Springer Verlag; 2006.

[20] Schulz F, Beyrau F. Systematic Investigation of Fuel Film Evaporation. SAE Technical Paper 2018-01-0310; 2018. https://doi.org/10.4271/2018-01-0310

[21] Kim H, Sung N. The effect of ambient pressure on the evaporation of a single droplet and a spray. Combust Flame 2003;135(3):261-70. https://doi.org/10.1016/S0010-2180(03)00165-2

[22] Tao M, Ge H, VanDerWege B, Zhao P. Fuel wall film effects on premixed flame propagation, quenching and emission. Int J Engine Res 2018. (Online First). https://doi.org/10.1177/1468087418799565